

Continuous Methane Emissions from the Oil and Gas Industry in the Permian Basin

Veefkind Joris Pepijn¹, Serrano-Calvo Raquel², de Gouw Joost A³, Dix Barbara Klara³, Schneising Oliver⁴, Buchwitz Michael⁴, Barré Jerome E⁵, van der A Ronald J.⁶, Liu Mengyao⁷, and Levelt Pieternel F⁸

¹Royal Netherlands Meteorological Institute (KNMI)

²Delft University of Technology, Dept. Geoscience and Civil Engineering

³University of Colorado Boulder

⁴University of Bremen

⁵National Center for Atmospheric Research (UCAR)

⁶KNMI

⁷Royal Netherlands Meteorological Institute

⁸National Center for Atmospheric Research

November 16, 2022

Abstract

Emissions of methane (CH_4) in the Permian basin (U.S.A.) have been derived for 2019 and 2020 from satellite observations of the Tropospheric Monitoring Instrument (TROPOMI) using the divergence method, in combination with a data driven method to estimate the background concentrations. The resulting CH_4 emission data, which have been verified using model with known emissions, have a spatial resolution of approximately 10 km. The spatial patterns of the emissions are in a good agreement with the locations of oil and gas production and drilling activities in the Permian basin, as well as with emissions of nitrogen oxides (NO_x). Analysis of time-series of locations with large CH_4 emissions indicated that there are significant continuous emissions in this region. The CH_4 emissions can be characterized as a continuous area source, rather than as dominated by a few large unplanned releases. This is important considering possible CH_4 emission mitigation strategies. In addition to providing spatially resolved emissions, the divergence method also provides the total emissions of the Permian basin and its main sub-basins. The total CH_4 emission of the Permian is estimated as $3.0 \pm 0.7 \text{ Tg yr}^{-1}$ for 2019, which agrees with other independent estimates based on TROPOMI data. For the Delaware sub-basin, it is estimated as $1.4 \pm 0.3 \text{ Tg yr}^{-1}$ for 2019, and for the Midland sub-basin $1.2 \pm 0.3 \text{ Tg yr}^{-1}$. In 2020 the emissions are 8% lower compared to 2019, which could be a result of strong decreases in drilling activities due to the COVID-19 crisis.

Continuous Methane Emissions from the Oil and Gas Industry in the Permian Basin

**J. P. Veefkind^{1,2}, R. Serrano-Calvo², J. de Gouw^{3,4}, B. Dix³, O. Schneising⁵, M. Buchwitz⁵,
J. Barré⁶, R. van der A¹, M. Liu¹, P.F. Levelt^{1,2,7}**

¹ Royal Netherlands Meteorological Institute KNMI, De Bilt, The Netherlands.

² Delft University of Technology, Dept. Geoscience and Civil Engineering, Delft, The Netherlands.

³ Cooperative Institute for Research in Environmental Sciences, University of Colorado, Boulder, CO, United States.

⁴ Department of Chemistry, University of Colorado, Boulder, CO, United States.

⁵ Institute of Environmental Physics (IUP), University of Bremen FB1, Bremen, Germany.

⁶ University Cooperation for Atmospheric Research, Boulder, CO, United States.

⁷ National Center for Atmospheric Research, Boulder, CO, United States.

Corresponding author: Pepijn Veefkind (pepijn.veefkind@knmi.nl)

Key Points:

- Methane emissions from the Permian basin in the U.S.A. can be derived from satellite data with a spatial resolution of approximately 10 km.
- The derived emissions are spatially consistent with satellite derived NO_x emissions and oil and gas industry activities.
- The dominant fraction of the methane emissions is from continuous emissions by the oil and gas industry.

Abstract

Emissions of methane (CH_4) in the Permian basin (U.S.A.) have been derived for 2019 and 2020 from satellite observations of the Tropospheric Monitoring Instrument (TROPOMI) using the divergence method, in combination with a data driven method to estimate the background concentrations. The resulting CH_4 emission data, which have been verified using model with known emissions, have a spatial resolution of approximately 10 km. The spatial patterns of the emissions are in a good agreement with the locations of oil and gas production and drilling activities in the Permian basin, as well as with emissions of nitrogen oxides (NO_x). Analysis of time-series of locations with large CH_4 emissions indicated that there are significant continuous emissions in this region. The CH_4 emissions can be characterized as a continuous area source, rather than as dominated by a few large unplanned releases. This is important considering possible CH_4 emission mitigation strategies. In addition to providing spatially resolved emissions, the divergence method also provides the total emissions of the Permian basin and its main sub-basins. The total CH_4 emission of the Permian is estimated as $3.0 \pm 0.7 \text{ Tg yr}^{-1}$ for 2019, which agrees with other independent estimates based on TROPOMI data. For the Delaware sub-basin, it is estimated as $1.4 \pm 0.3 \text{ Tg yr}^{-1}$ for 2019, and for the Midland sub-basin $1.2 \pm 0.3 \text{ Tg yr}^{-1}$. In 2020 the emissions are 8% lower compared to 2019, which could be a result of strong decreases in drilling activities due to the COVID-19 crisis.

Plain Language Summary

Methane is a strong greenhouse gas that contributes to climate change. One of the main emissions sources of methane is from the oil and gas industry. To be able to reduce these emissions we have to know the main sources and monitor if reduction measures work. In this study we estimated the emissions for the Permian basin in the U.S.A. using satellite observations. This provides us with maps of the emissions with a spatial resolution of 10 km. The results indicate that continuous emissions are important in the Permian basin. This may be caused by small emissions from the thousands of wells in the Permian basin. Also, we were able to estimate the annual emissions from the basin, which correspond well with other studies.

1. Introduction

Methane (CH_4) is the second most important greenhouse gas after CO_2 . As the atmospheric lifetime of CH_4 is relatively short at 9.1 years and the global warming potential large, a reduction in CH_4 emissions would lower the combined radiative forcing from greenhouse gases on a timescale of years and is therefore a relatively efficient option to mitigate climate change. For this reason, the Global Methane Pledge was initiated at the UN Climate Change Conference (COP26) in November 2021 [*European Commission, United States of America*, 2021], which aims at reducing CH_4 emissions by 30% in 2030.

A significant fraction of global methane emissions comes from the oil and gas (O&G) industry [*IEA*, 2021]. CH_4 is emitted during the construction of new wells, when operating wells, during storage and transportation of oil and gas, and when wells are abandoned. Some of the emissions are intended releases, for example from venting, others are unintentional and caused by malfunctioning equipment or by accidents. To be able to effectively reduce CH_4 emissions from the O&G industry, the largest contributions must be known, and which ones can be mitigated with the least effort. In the recent literature there has been a strong focus on the detection of large emissions (aka super-emitters) in O&G production regions using satellite data [*Cusworth et al.*, 2021; *Irakulis-Loitxate et al.*, 2021; *Lauvaux et al.*, 2022], for example in Turkmenistan [*Irakulis-Loitxate et al.*, 2022] and Algeria [*Varon et al.*, 2021]. In this paper we focus on the Permian basin, which is the largest oil and gas producing region in the U.S.A. The Permian basin is located in Texas and New Mexico and covers an area of approximately 160,000 km^2 . The exploitation of the Permian basin is mostly done using non-conventional technologies, including hydraulic fracturing and horizontal drilling. The area is characterized by thousands of production facilities and new ones are continuously developed, while others are abandoned when no longer productive. Observations from the ground [*Robertson et al.*, 2020], from aircraft and satellites have shown significant emission of CH_4 , but also other gases like nitrogen dioxide (NO_2) and formaldehyde [e.g. *de Gouw et al.*, 2020]. For reducing the CH_4 emissions, a key question is if these emissions are dominated by a few large point sources, or caused by many small emissions, which together form a continuous area source. This is important because large emissions from a few facilities will be easier to reduce than small emissions from many facilities [*Mayfield et al.*, 2017]. We address this question using satellite data from the Tropospheric Monitoring Instrument (TROPOMI) on board of the European Sentinel 5 Precursor (S5P)

satellite [Veeffkind *et al.*, 2012], which was launched in 2017. The CH₄ observations of TROPOMI have a spatial resolution of approximately 7x5.5 km² in nadir and larger towards the edges of the 2600 km wide swath. The main contribution of TROPOMI for CH₄ emission monitoring is the continuous mapping capability, providing a large number of overpasses over any given region on Earth. The spatial resolution is not sufficient to detect the frequent but relatively small individual plumes in the Permian. Instead of detecting individual plumes, the aim of this work is to derive CH₄ emissions on a spatial resolution of approximately 10 km. TROPOMI data have been used for quantifying emissions for the Permian basin using the wind rotation method [Schneising *et al.*, 2020], Bayesian inversion involving chemistry-transport modelling [Zhang *et al.*, 2020] and the divergence method [Liu *et al.*, 2021]. The emission estimates of these studies are in the range of 2-4 Tg yr⁻¹ CH₄ for the period 2018-2019.

In this work, we use the divergence method with a new data-driven approach to derive the large CH₄ background column, which removes the need for model estimates of the background. Before applying it to satellite data, we verify the method using model data. The spatial distribution of the TROPOMI derived emissions is compared to oil and gas production and drilling information and with TROPOMI derived NO_x emissions. A time series analysis for locations in the Permian basin with large emissions is presented, as well as the estimate of the emissions of the entire Permian basin.

2. Materials and Methods

In this section we describe the methods that are used to derive emissions from the column-averaged dry air mole fraction of methane (XCH₄). This involves two steps: first the CH₄ background and the enhanced column densities are computed, next the divergence is applied to estimate the emissions.

2.1 Background correction

The background correction first converts the XCH₄ volume mixing ratio into the CH₄ concentration, n , in units of mole m⁻², by multiplying with the dry air number density:

$$n = 10^{-9} \text{XCH}_4 \frac{p_{sfc}}{g m_{air}} \quad \text{Equation 1}$$

where n is the CH_4 concentration in units of mole m^{-2} , p_{sfc} is the surface pressure in Pa, g is gravitational constant, estimated as $9.81 \text{ m}^2 \text{ s}^{-1}$, and m_{air} is the molar mass of dry air ($28.9647 \text{ g mole}^{-1}$).

Since this study focuses on a small domain, the daily transport in the upper atmosphere, which was estimated by the daily model re-analysis in Liu et al. (2021) can be simplified. To estimate the background CH_4 concentration, a simple model is applied that describes the CH_4 column concentration as the sum of a stratospheric contribution, a background tropospheric concentration and a lower tropospheric enhancement. This model is illustrated in Figure 1, which shows model data for a profile with and without lower tropospheric enhancement. The bulk of the CH_4 column is determined by the tropospheric background, for which the concentration is almost constant from the surface to the tropopause ($\sim 100 \text{ hPa}$ for this profile). The concentration in the stratosphere decreases strongly with altitude. For the example shown in Figure 1, the contribution of the lower tropospheric enhancement contributes 1.4% to the column integrated XCH_4 .

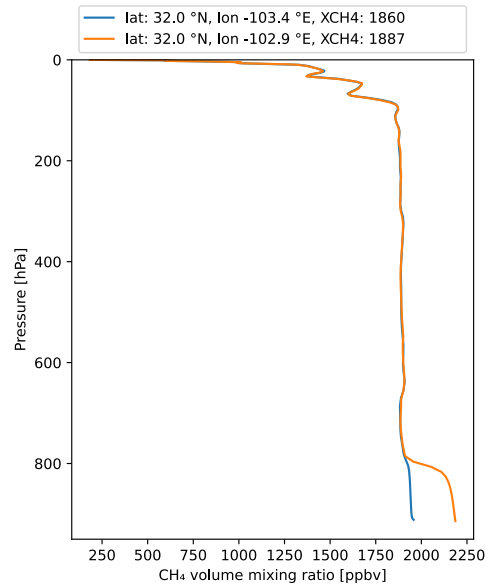


Figure 1. CAMS model (see section 3) CH_4 volume mixing ratio profiles for two nearby locations for 1 October 2020. The blue line represents background conditions and the orange line enhanced CH_4 concentrations in the lower troposphere.

Using the model described above, the CH_4 column concentration can be written as:

$$n = k X\text{CH}_4_s p_{tp} + k X\text{CH}_4_t (p_{sfc} - p_{tp}) + \Delta n \quad \text{Equation 2}$$

where $k = \frac{10^{-9}}{g m_{air}}$, $X\text{CH}_4_s$ is the mean CH_4 concentration in the stratosphere, $X\text{CH}_4_t$ is the mean CH_4 concentration in the troposphere, p_{tp} is the tropopause pressure and Δn is the lower tropospheric CH_4 enhancement.

For a limited-sized area we assume that the tropopause pressure, $X\text{CH}_4_s$ and $X\text{CH}_4_t$ are constant over the area, whereas Δn is expected to vary. Although stratospheric intrusions are common in the western U.S. [e.g. Lin et al., 2012], especially in spring, the Permian basin is at the eastern end of the affected area and therefore the impact of the assumption of a constant tropopause pressure will hold on most days. Under these assumptions, Equation 2 can be rewritten as:

$$\Delta n = n - (c_0 + c_1 p_{sfc}) \quad \text{Equation 3}$$

where $c_0 = k (X\text{CH}_4_s - X\text{CH}_4_t) p_{tp}$ and $c_1 = k X\text{CH}_4_t$.

Thus, the background can be estimated by linearly fitting the CH_4 concentration n as function of the surface pressure p_{sfc} , yielding the constants c_0 and c_1 . This is expected to provide an accurate estimate of the background CH_4 concentration when the lower tropospheric enhancement Δn is close to zero for the larger part of the area. To make the fit less sensitive to the enhanced CH_4 concentration values, we first bin the data based on the surface pressure. For each bin we compute the 25th percentile of the CH_4 concentration and the median surface pressure. These binned points are fitted using a linear least-squares fit, yielding the parameters c_0 and c_1 of Equation 3, which describe the background CH_4 column concentration.

The method to estimate the background column concentration and the lower tropospheric enhancement is illustrated in Figure 2 over the Permian region for 6 October 2020. In the figure the CH_4 column concentration is shown along with the linear fit. A number of pixels significantly exceed the background concentration, which is represented by the line. The images show the constructed background column concentration and the background corrected CH_4 column (Δn). It is noted that Δn will show similar spatial features as XCH_4 , however it is now in number density units, required for the divergence method.

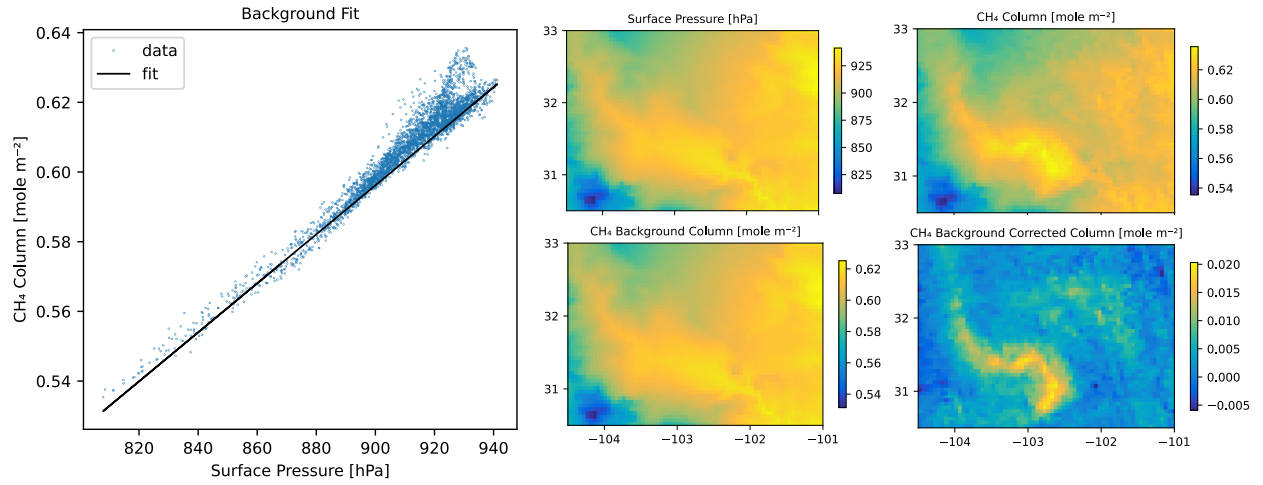


Figure 2. Illustration of the background correction for data over the Permian region for 6 October 2020. Left panel: CH_4 column concentration plotted as function of the surface pressure (blue points) and the corresponding linear fit (black line). Middle top panel: surface pressure. Right top panel: CH_4 column concentration. Middle bottom panel: background CH_4 column concentration. Right bottom: background corrected CH_4 column concentration.

2.2 Divergence Method

Based on the conservation of mass, the emission can be computed as the horizontal flux divergence [Beirle et al., 2019], assuming that the sink term can be neglected due to the long atmospheric lifetime of CH_4 [Liu et al., 2021]. From the continuity equation for steady state conditions, the emission can be computed as:

$$E = \frac{\partial \Delta n_x u}{\partial x} + \frac{\partial \Delta n_y v}{\partial y} \quad \text{Equation 4,}$$

where x and y are the two perpendicular horizontal directions and $v=(u,v)$

The divergence is computed using numerical derivatives calculated as the fourth-order or second-order central-finite difference. The divergence method is extended here by introducing a second estimate of the divergence. As illustrated in Figure S1, the standard divergence method computes the divergence based on pixels in the S-N and E-W direction. While this method already has proven very powerful, it doesn't make full use of the observations. A second estimate of the divergence can be computed by using the ground pixels in the SW-NE and NW-SE direction (the orange pixels in Figure S1). We compute the wind vector (u', v') on these axes, by applying a rotation of 45° with respect to the original wind vector (u, v). This provides two estimates of the divergence, which are combined by computing a weighted average. The weight depends on the wind direction and is computed for each grid box: when the wind is along the SN or EW direction, more weight is given to the original divergence, and when the wind is in the SW-NE or NW-SE direction more weight is given to the rotated divergence. The weight of the SN-EW direction is given by:

$$w_0 = \left| \frac{\varphi}{45} - 1 \right| \quad \text{Equation 5,}$$

where φ is the angle in degrees between the vectors (u, v) and ($\bar{u}, 0$). The weight for the NW-SE direction is $1 - w_0$.

Including the second estimate of the divergence has two advantages: firstly, it increases the data coverage because one of the divergence values maybe missing due to missing or invalid input data, secondly it potentially reduces the noise, because we use twice as much data to compute the divergence.

Figure S2 illustrates the full workflow that has been developed. The daily XCH₄ mixing ratios are background corrected yielding the tropospheric enhancements number densities. Filtering is applied to remove grid boxes for which the terrain height is varying strongly, as the background correction is expected to be inaccurate for these conditions. Additionally, this step avoids the posterior correction on the background correction, which is important in Liu et al., (2021). The tropospheric enhancements are used by the divergence method to compute daily CH₄ emissions. As a default we use a boundary layer height of 500m for averaging of the wind and compute the divergence using a fourth-order finite difference. The daily emissions are filtered to only include grid boxes which have valid neighbors to remove effects of cloud edges. Mean and

median emissions are computed from the daily data for the years 2019 and 2020 and for the entire period.

3. Data

S5P TROPOMI CH₄ mixing ratios are from the Weighting Function Modified Differential Optical Absorption Spectroscopy (WFM-DOAS) algorithm version 1.5 [Schneising *et al.*, 2019]. The main data fields used are the methane column-averaged dry air mole fraction (XCH₄), the surface pressure, the geolocation and the data quality information. The WFMD-DOAS data were downloaded from https://www.iup.uni-bremen.de/carbon_ghg/products/tropomi_wfmd for the years 2019 and 2020.

From the global data, a daily gridded dataset for the years 2019 and 2020 is derived on an equirectangular grid with a resolution of 0.05° in both latitude and longitude, which corresponds to 5.5 km in the N-S direction and for a latitude of 30° to 6.4 km in the E-W direction. Note that the resolution is similar to the nadir resolution of the TROPOMI CH₄ observations (5.5 km in flight direction and 7 km in the cross-flight direction). The gridding processing uses the ground pixel corners provided to calculate the overlap with the grid boxes, which are used to compute weighted averages. The gridding yields daily fields of XCH₄ and surface pressure. Only ground pixels with the recommended data quality are included in the gridded fields.

Meridional and zonal wind components are from the ERA-5 reanalysis from the European Centre for Medium-Range Weather Forecasts [Hersbach *et al.*, 2020]. The wind data is downloaded for all 14 pressure levels between 600 and 1000 hPa and has a spatial resolution of 0.25° x 0.25° latitude/longitude and an hourly temporal resolution. In the divergence method we take the wind history into account by averaging the wind data for the time steps of 17, 18 and 19 hrs UTC.

Model XCH₄ and surface pressure data have been used from the Copernicus Atmosphere Monitoring Service (CAMS) global forecasting system (IFS cycle 47R1) [Agustí-Panareda *et al.*, 2019], experiment he9h [Barré *et al.*, 2021]. These data include an adjustment of the concentrations using satellite data assimilation, whereas the emissions and surface fluxes remain unchanged by the satellite data assimilation procedure. Due to their respective vertical sensitivities, the satellite data mainly provide a correction to the concentrations in the free

troposphere and above. At lower altitudes, the emissions are the dominant influence on CH₄ concentration. The CAMS data have a spatial resolution of 0.1° x 0.1° latitude x longitude. Data for each day of the year 2020 at 18:00 UTC were obtained and resampled to the same spatial grid as the TROPOMI XCH₄ data. Also, all grid boxes for which the TROPOMI data has fill values were removed in the CAMS XCH₄ data set, to generate representative pseudo-observations. In addition to the CAMS XCH₄ data, the CAMS emissions version 4.2 with a spatial resolution of 0.1° x 0.1° latitude x longitude have been used [Granier *et al.*, 2019]. The anthropogenic emissions in this data set, including fossil fuel, agricultural and landfill/waste emissions, are from EDGARv4.2FT2010 [Olivier and Janssens-Maenhout, 2012]. From the original monthly data, average emissions for the sum of all sectors for 2019 and 2020 have been constructed.

Oil and gas production data and drill rig counts are from the Enverus Drilling Info and Rig Analytics data base tools (<https://www.enverus.com/drillinginfo-and-rigdata/>, last accessed 25-2-2022), respectively. Oil and gas production volumes are reported monthly for each well location and gridded to match the TROPOMI CH₄ maps. The locations of drill rigs are reported daily. Monthly gridded maps are created by counting the number of drill rigs within each grid cell weighted by the number of days on location per month.

The NO_x emission data are from [Dix *et al.*, 2022]. These data represent a mean NO_x emission for the time period May 2018 until December 2020. The data have been regridded to the same latitude-longitude grid as the TROPOMI XCH₄ data.

4. Verification using CAMS model data

The divergence method has been verified using CAMS model data, for which the input emissions are known. As described above, the CAMS data for 2020 were gridded and sampled for the grid boxes for which also TROPOMI XCH₄ is available. Thus, it has the same coverage as the TROPOMI, including missing data due to for example cloud contamination. On this dataset we apply the same background correction and derive the emissions using the divergence method. Figure 3 shows the median emission for 2020 derived from the CAMS data as well as the input emissions. The retrieved emissions show generally the same spatial features as the input emissions, however at a lower spatial resolution. To test this, we applied a Gaussian blur to the input emissions. We manually varied the standard deviation σ of the Gaussian kernel and found that for a value of approximately 9 km the resolution of the retrieved and input emissions

match well. The spatial resolution has a strong effect on the slope between the retrieved and input emissions, and the correlation coefficient increases from 0.75 to 0.93 when the Gaussian blur is applied. Whereas the divergence method favorably retrieves the spatial variability of the emissions, retrieving the total emission is more complicated. We computed the total emission for the Delaware and Midland sub-basins, as well as for the entire Permian basin (the definition of these regions is shown in *Figure S3*). The estimated emission for the Delaware sub-basin shows a bias of -16% lower compared to the CAMS inputs, for the Midland sub-basin -40% and for the entire Permian basin -42%. The total emission estimates are sensitive to a possible offset: applying an offset of $1.0 \text{ kg km}^{-2} \text{ hr}^{-1}$ to the retrieved emissions is sufficient to close the gap between the retrieval and the input. The bias with this offset applied is 7%, -8% and -1%, for the Delaware sub-basin, the Midland sub-basin and the entire Permian basin. The mean emission of the Delaware sub-basin is almost a factor of 2.0 larger compared to the mean for the entire Permian basin. For the Midland basin this is a factor of 2.6. For larger emissions, a bias will have a smaller relative impact than for lower emissions. This agrees with the finding that the bias is lower for the Delaware sub-basin. Thus, these results point to a possible low bias of the method, which is a potential limitation of the method for estimating the total emission of a region, especially when the average emissions are small. A possible complication of this analysis is that in the CAMS dataset the concentrations and emissions are not consistent, because only the concentrations are adjusted using satellite observations. However, it is not straightforward to assess the sign or magnitude that this may have on the emissions derived with the divergence method.

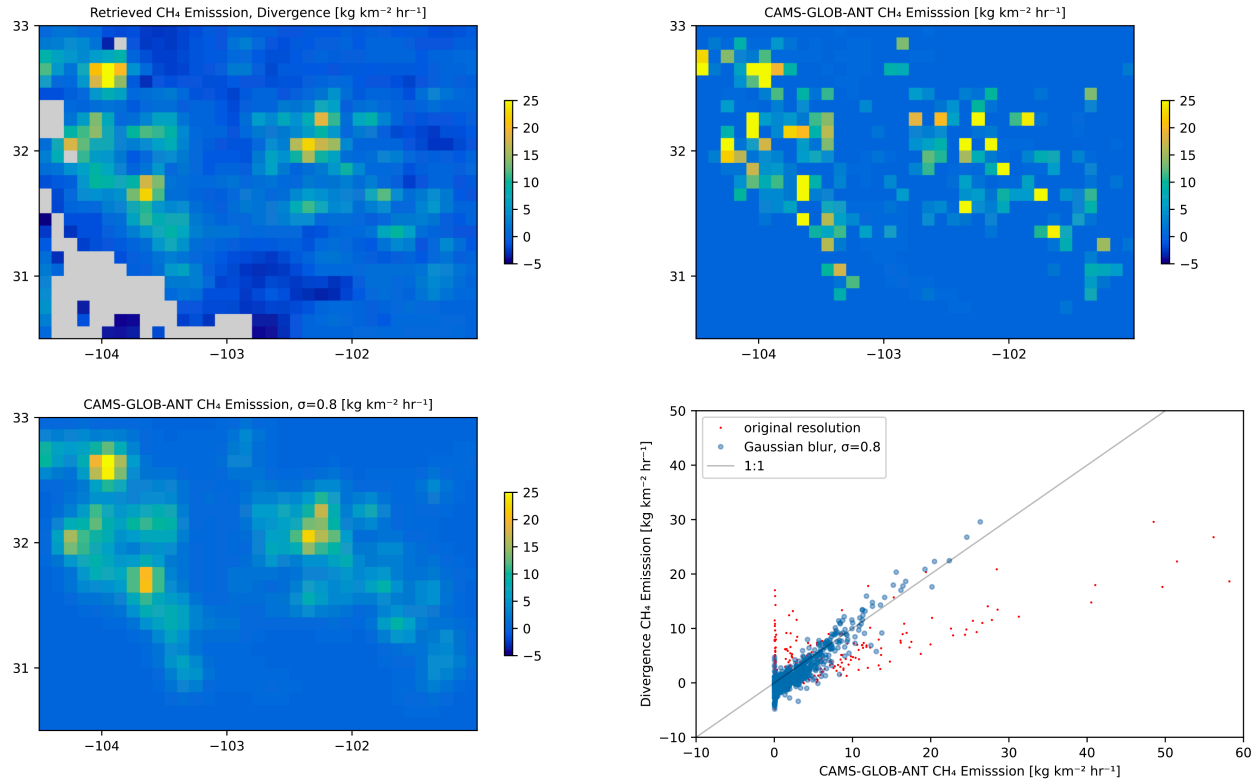


Figure 3. Divergence method applied to CAMS model data. Top-left panel: CH_4 emission derived from CAMS model data with the divergence method. Top-right panel: CAMS input emissions on the original resolution. Bottom-left panel: CAMS input emission with a Gaussian blur with $\sigma=0.8$. Bottom-right panel: retrieved emissions plotted as function of the CAMS input emissions, for the original and blurred data.

The CAMS data have also been used to test the sensitivity for variations in the setup. The default divergence setup uses a boundary layer height of 500 m and a fourth-order central-finite difference method for calculating the derivatives. We have tested the impact of boundary layer heights of 250 and 1000 m, the use of second-order central-finite difference, and the use of a least-squares fit (instead of the fit based on the 25th percentile) to compute the background. The boundary layer height is important because the wind is computed as the mean over this layer. As can be seen in Table 1, the largest impact on the mean emission is due to the background method (-19% compared to the default) and increasing the boundary layer to 1000 m (-11%). The impact of changing the boundary layer to 250 m and the impact of the central-finite difference method order is marginal (<2%). These results are similar to the results presented in [Liu et al., 2021].

Based on this sensitivity analyses, we estimate the uncertainty of the mean emissions of the order 25%.

Emission [$\text{kg m}^{-2} \text{ hr}^{-1}$]	Default	250 m	1000 m	2 nd order	Ltsq
Mean	1.44	1.47	1.28	1.43	1.17
Median	0.16	0.23	0.01	0.21	-0.20
P1	-0.90	-0.84	-1.04	-0.85	-1.08
P3	2.20	2.19	2.10	2.24	1.90

Table 1. Sensitivity of the emissions for 2020 derived from the CAMS data for the entire domain, for variations in the assumed boundary layer height, the order of the central-finite difference method and the method to compute the background. The first column represents the default case, which uses a boundary layer height of 500m, 4th order central finite difference and a fit of the background concentration based on the 25th percentiles. Variations with respect to the default are a 250 m or 1000m boundary layer height, a 2nd order the central-finite difference method, and a least-squares fit (Ltsq) for the background concentration. The table lists the mean, median, 25th percentile (P1) and 75th percentile (P3) of the difference with the default case.

5. CH₄ derived from TROPOMI Data

The median CH₄ emissions derived by applying the divergence method to TROPOMI WFMD data for 2019-2020 are shown in *Figure 4*. Overall, the emission is highest in regions where there are activities related to the O&G industry. The spatial outline of the Delaware and Midland sub-basins can be distinguished clearly in this figure. Whereas the main outlines correspond to the emission data derived from the CAMS model data (*Figure 3*, top left panel), there are significant differences between these maps. The TROPOMI results show significantly higher spatial variability. This may be caused by the instrument noise, which is not accounted for in the CAMS analysis. In addition, the CAMS model assumes a fixed pattern, whereas in reality, the emissions will vary significantly in space and time. Also, for the CAMS data the wind information and the advection in the model are consistent, whereas for the application on TROPOMI data there may be significant errors in the wind fields. Some regions in *Figure 4* show negative emissions, which are considered artefacts of the method. In regions with significant variability in orography, the assumed vertical model (Equation 2) may not hold, leading to such artefacts.

316 The NO_x emissions in the Permian basin are to a large extent related to the O&G
317 industry. Although the NO_x emissions come from different sources, mainly generators and
318 engines, they are expected to come from the same sites as where the CH₄ is emitted [*Warneke et*
319 *al.*, 2014]. The NO_x and CH₄ emissions derived from TROPOMI (*Figure 4*) show similar spatial
320 variations. The spatial correlation is higher in the western Delaware basin. NO_x also has
321 significant contributions from road transportation and power generation. In the NO_x emission,
322 spatial features related to the main cities, Midland and Odessa and the Interstate I-20 can be
323 distinguished [*Dix et al.*, 2022]. As expected, these features are not found in the CH₄ emission
324 data.

325 To further link the satellite derived CH₄ emission data with the O&G industry activities,
326 we used data on the oil and gas production and on the drilling days. For each grid box we define
327 a score of 0-3 for oil production, gas production and drilling. A score of 0 is given when the
328 activity data are less than 1% of the median, a score of 1 when the data are higher than this value
329 but less than the 25th percentile, a score of 2 when the data are between the 25th and 75th
330 percentile, and a score 3 when the data are higher than the 75th percentile. Finally, the scores of
331 oil production, gas production and drilling are combined, which gives 10 categories ranging from
332 0 to 9. The map of the categories and the distribution of the CH₄ emissions over the categories
333 are shown in *Figure 4*. As can be seen in the figure, the overall spatial variation of the production
334 and drilling data shows good agreement with both the CH₄ and NO_x emissions. Especially for the
335 categories 7-9 significantly higher CH₄ and NO_x emissions are found. The lower categories show
336 an average value of near zero, which is also a sign that the satellite retrievals are in
337 correspondence with the oil and gas activity data.

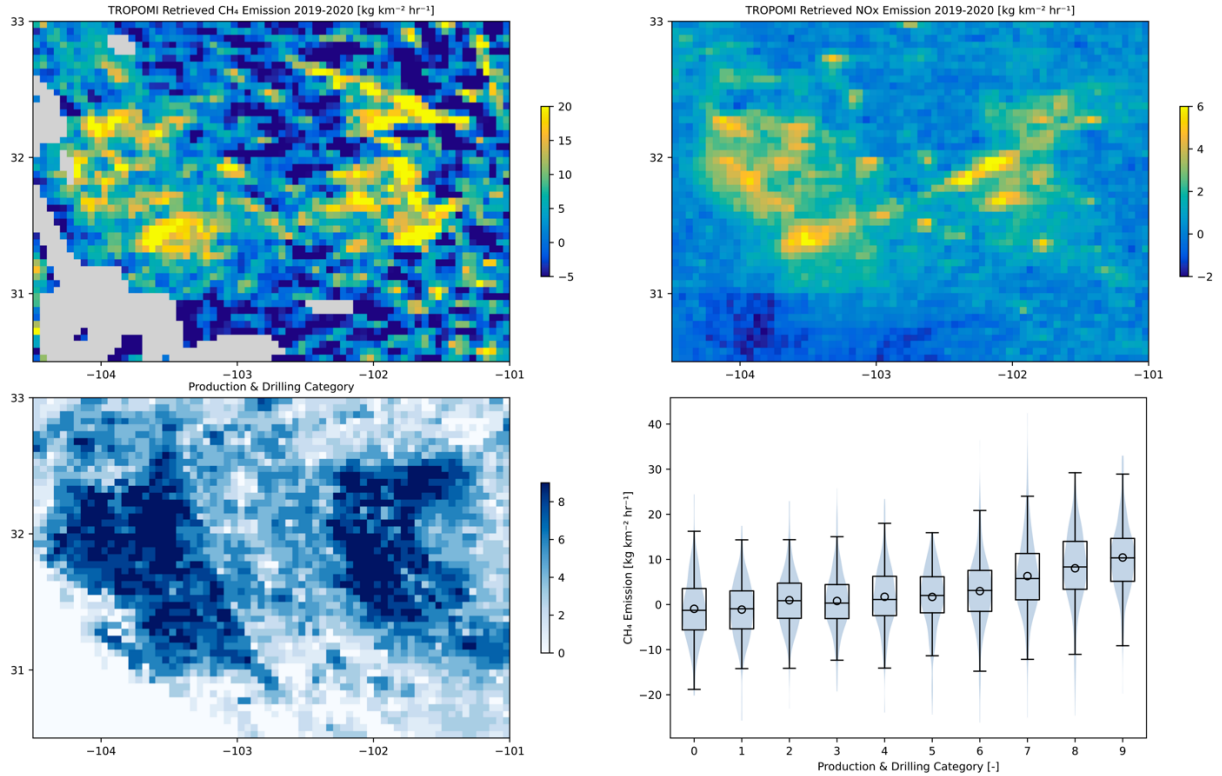


Figure 4. Panel top left: Median CH_4 emission derived using the divergence method applied to TROPOMI data from 2019-2020. Top-right NO_x emission for 2018-2020 retrieved from TROPOMI [REF Dix]. Bottom left: production drilling categories. Bottom right, combined violin and boxplot showing the distribution of retrieved CH_4 emissions for each production/drilling category.

For five locations with high median emissions, labeled A to E in Figure S3, a time series of the CH_4 emission for 2019 and 2020 are shown in Figure 5. These five locations have been selected by hand from the median emission map (Figure S3). For all locations, except for location C, the 30-day running mean and 30-day running median are above zero for almost the entire time period. As can be seen in Figure S3, there is an area with negative median emissions just north of the location C. These negative emissions are probably an artefact of the orography and are also affect the time series for the location C. For all five locations in Figure 5 the mean emission over the whole time period is larger than the median value, indicating that the distribution is skewed towards the larger values. Although the mean value is much more sensitive to outliers compared to the median, the mean falls well in the interquartile range. Furthermore, the difference between the mean and median is less than 30% for the five locations.

355 The median value is more representative for the continuous emissions and less sensitive to
356 extreme values compared to the mean. For reference, *Figure S4* shows a similar plot as *Figure 5*,
357 but for five locations with background emission values. For these background locations the
358 difference between the mean and median over the entire time period is smaller as compared to
359 the locations with high emissions.

360 We also analyzed the distribution of the daily emissions for the Permian basin and the
361 sub-basins. Overall, the distributions are heavy tailed and skewed towards the large values. For
362 the 2019-2020 period the mean is 30% higher than the median for the entire Permian and 24%
363 and 27% for the Delaware and the Midland sub-basins.

364 Super emitting events that are short in duration will have a much larger effect on the
365 mean than on the median. The fact that the mean and median differ by less than 32% for both the
366 time series for high emitting locations as well as for the entire Permian basin, indicates that a
367 large fraction of the emissions is continuous rather than episodic. This is further supported by the
368 inspection of monthly maps, which show similar spatial patterns of the main CH₄ emission
369 hotspots.

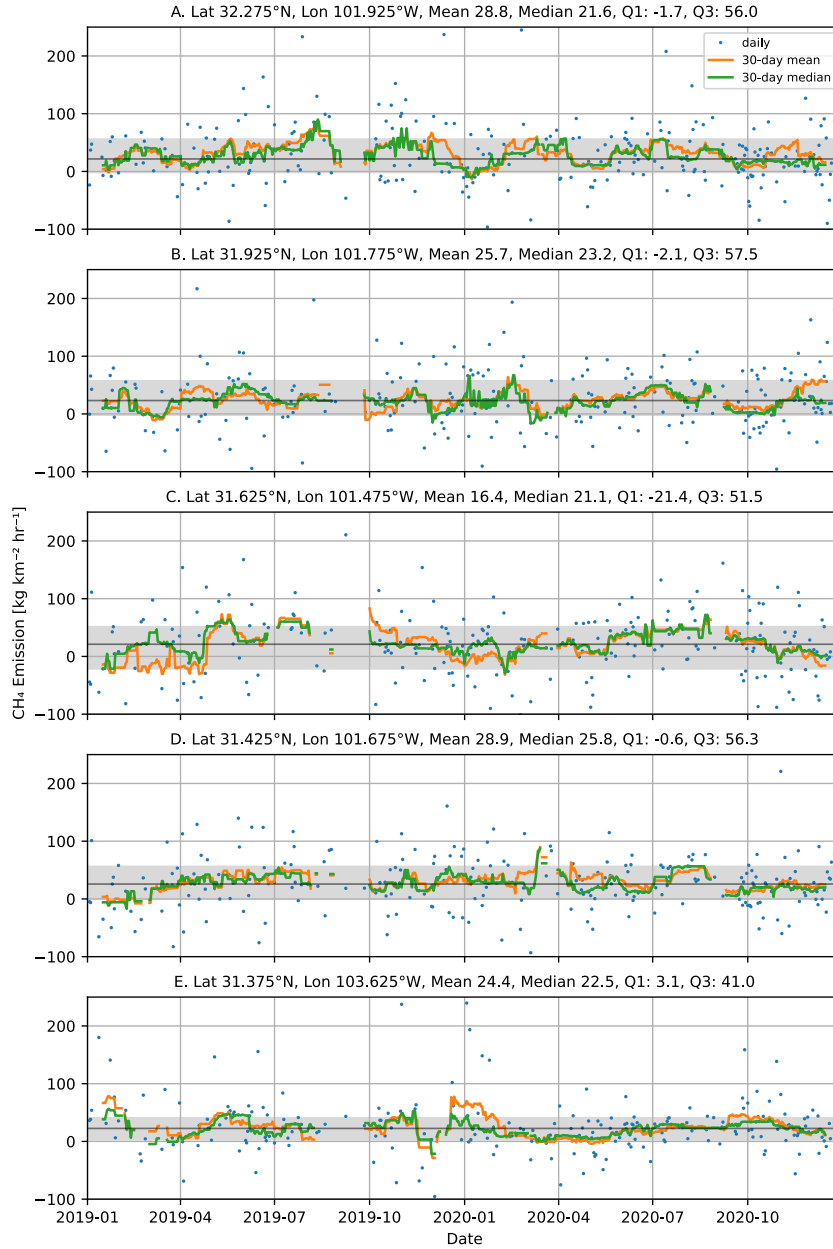


Figure 5. Time series for five locations with high CH₄ emissions. The blue dots are the daily data, the orange line the 30-day running mean and the green line represents the 30-day running median. Running mean and medians are only shown when at least 5 of the 30 days contain valid data. The grey area indicates the interquartile range and the black line the median over the whole time period.

From the daily emissions we estimated the annual emissions for three regions: the Delaware sub-basin, the Midland sub-basin and the entire Permian. The boundaries used for the

Delaware and Midland basin are shown in *Figure S3*, the Permian basin covers the entire map. The annual emissions were calculated by summing the yearly mean values of a basin and were converted to Tg yr^{-1} . The derived annual emissions are listed in *Table 2* for 2019, 2020 and 2019-2020. Based on the sensitivity analysis presented in Section 2, we estimate the uncertainty in these numbers as 25%. This uncertainty is dominated by biases caused by the configuration of the method. Therefore, the uncertainties in the annual emissions are expected to be significantly larger compared to differences in the annual emissions between the years.

The annual CH_4 emissions of the Delaware and the Midland basin are found to be comparable. It is estimated that these sub-basins contribute 70-90% to the entire CH_4 emissions of the Permian basin. The derived emissions are found to be 8 to 27 % lower in 2020 compared to 2019, which could be an indication of the impact of the COVID-19 crisis [*Lyon et al.*, 2021].

Table 2. Annual Emissions derived with the divergence method for the Delaware, Midland sub-basins and for the entire Permian basin for 2019, 2020 and 2019-2020. The Delaware and Midland basins are sub-basins of the Permian (see Figure S3).

Annual Emission [Tg yr^{-1}]	Delaware	Midland	Permian
2019	1.4	1.2	3.0
2020	1.1	0.9	2.7
2019-2020	1.3	1.0	2.9
Difference 2020 - 2019	-18%	-27%	-8%
Estimated 1- σ uncertainty of the emission is 25%			

6. Conclusions

We have investigated the CH_4 emissions from the oil and gas industry in the Permian basin for 2019 and 2020 using satellite data. We used the divergence method to derive daily CH_4 emissions. Compared to previous applications of the divergence method for CH_4 emissions [*Liu et al.*, 2021], we applied a model-independent correction to derive the CH_4 background concentration. This method assumes that the background CH_4 concentration in the troposphere

and the tropopause height is spatially constant and is therefore limited to regional applications. Using model data for 2020 we demonstrated that the divergence method can retrieve the spatial variability of the emissions at a reduced spatial resolution of approximately $10 \times 10 \text{ km}^2$. Based on a sensitivity analyses, we estimate that the uncertainty in the yearly mean emissions is of the order 25%.

The divergence method to TROPOMI CH_4 data was applied for the years 2019-2020: The spatial patterns between these years agree well, indicating that the method gives consistent results. The spatial distribution shows generally the same structures as oil and gas activity data (production and drilling) and NO_x emissions, also derived using TROPOMI. However, there is a weak spatial correlation between the CH_4 emissions and the activity and NO_x emissions. Therefore, constructing CH_4 emissions from these data sets, as suggested by [de Gouw *et al.*, 2020] will require additional information, for example locally varying conversion factors. The spatially variability of the retrieved emissions differs clearly from the CAMS emission data set [Granier *et al.*, 2019].

Time series for locations with high CH_4 emissions and background values were analyzed. The background locations have near zero or negative median emissions over the time series. The interquartile range in the data is typically $40 \text{ kg km}^{-2} \text{ hr}^{-1}$. The time series of high emission locations shows for four out of five locations a skewed distribution towards higher values. However, the difference of the mean and median over the time series differ less than 32%, indicating that the mean value is not dominated by a few outliers. From this analysis we speculate that the emissions in the Permian basin are driven by continuous emissions, rather than by a few large unplanned releases. This is important, because it means that the emissions may be caused by the daily operations and given the large number of facilities in the Permian, they may be hard to reduce. The continuous emission was also found by [Schneising *et al.*, 2020] for the entire Permian basin, and here we confirm that this also applies to spatially resolved data,

The total emissions were estimated for the Delaware and Midland basins and for the entire Permian basin. For the entire basin we find values $3.0 \pm 0.7 \text{ Tg yr}^{-1}$ for 2019, For the Delaware basin we find emissions of $1.4 \pm 0.3 \text{ Tg yr}^{-1}$ and for the Midland basin $1.2 \pm 0.2 \text{ Tg yr}^{-1}$. The estimated 25% uncertainty is based on a sensitivity analysis of the retrieval method. The estimated emission for the Permian basin agrees within the uncertainties with estimates from

[Liu *et al.*, 2021] (2.82 to 3.78 Tg yr⁻¹), [Schneising *et al.*, 2020] (3.18±1.13 Tg yr⁻¹ for 2018-2019) and [Zhang *et al.*, 2020] (2.9±0.5 Tg yr⁻¹ for March 2018 – March 2019).

Annual emissions in the Permian basin for the year 2020 are 8% to 27% lower compared to 2019. Updated results using the method of [Schneising *et al.*, 2020] using the same data version as used in this work, show agreement for 2019 (2.92 +/- 1.61 Tg yr⁻¹), 2020 (2.27 +/- 1.75 Tg yr⁻¹) and confirm the reduction in emission in 2020 compared to 2019. A possible explanation is the drop in demand for oil and gas, leading to significantly reduced drilling activity and reduced production in the Permian basin in 2020.

Acknowledgments

The KNMI contributions to this research have been funded by the Netherlands Space Office, as part of the TROPOMI Science Contract. The contributions of the TU-Delft were funded by Shell Global Solutions International B.V. The contributions of the University of Bremen received funding from the European Space Agency (ESA) via the projects GHG-CCI+ and Methane+. The TROPOMI/WFMD retrievals were performed on HPC facilities of the IUP, University of Bremen, funded under DFG/FUGG grant INST 144/379-1 and INST 144/493-1.

This publication contains modified Copernicus Sentinel data (2019,2020). Sentinel-5 Precursor is an ESA mission implemented on behalf of the European Commission. The TROPOMI payload is a joint development by the ESA and the Netherlands Space Office (NSO). The Sentinel-5 Precursor ground-segment development has been funded by the ESA and with national contributions from The Netherlands, Germany, and Belgium.

Open Research

The main data sets that are used in this research are:

- The TROPOMI WFM-DOAS data available at https://www.iup.uni-bremen.de/carbon_ghg/products/tropomi_wfmd/
- The ERA-5 meteorological information available at <https://www.ecmwf.int/en/forecasts/datasets/reanalysis-datasets/era5>
- The CAMS model data are available from ECMWF.

Upon publication all Python scripts and data files used to generate and analyze the data will be made available for public access.

References

- Agustí-Panareda, A. et al. (2019), Modelling CO_2 weather – why horizontal resolution matters, *Atmospheric Chemistry and Physics*, 19(11), 7347–7376, doi:10.5194/acp-19-7347-2019.
- Barré, J. et al. (2021), Systematic detection of local CH_4 anomalies by combining satellite measurements with high-resolution forecasts, *Atmospheric Chemistry and Physics*, 21(6), 5117–5136, doi:10.5194/acp-21-5117-2021.
- Beirle, S., C. Borger, S. Dörner, A. Li, Z. Hu, F. Liu, Y. Wang, and T. Wagner (2019), Pinpointing nitrogen oxide emissions from space, *Science Advances*, 5(11), eaax9800, doi:10.1126/sciadv.aax9800.
- Cusworth, D. H. et al. (2021), Intermittency of Large Methane Emitters in the Permian Basin, *Environmental Science & Technology Letters*, 8(7), 567–573, doi:10.1021/acs.estlett.1c00173.
- Dix, B., C. Francoeur, M. Li, R. Serrano-Calvo, P. F. Levelt, J. P. Veefkind, B. C. McDonald, and J. de Gouw (2022), Quantifying NO_x Emissions from U.S. Oil and Gas Production Regions Using TROPOMI NO_2 , *ACS Earth Space Chem.*, doi:10.1021/acsearthspacechem.1c00387. [online] Available from: <https://doi.org/10.1021/acsearthspacechem.1c00387>
- European Commission , United States of America (2021), *Global Methane Pledge*. [online] Available from: <https://www.ccacoalition.org/en/resources/global-methane-pledge> (Accessed 11 February 2022)
- de Gouw, J. A., J. P. Veefkind, E. Roosenbrand, B. Dix, J. C. Lin, J. Landgraf, and P. F. Levelt (2020), Daily Satellite Observations of Methane from Oil and Gas Production Regions in the United States, *Scientific Reports*, 10(1), 1379, doi:10.1038/s41598-020-57678-4.
- Granier, C. et al. (2019), *The Copernicus Atmosphere Monitoring Service global and regional emissions (April 2019 version)*, Copernicus Atmosphere Monitoring Service (CAMS) report. [online] Available from: doi:10.24380/d0bn-kx16
- Hersbach, H. et al. (2020), The ERA5 global reanalysis, *Quarterly Journal of the Royal Meteorological Society*, 146(730), 1999–2049, doi:https://doi.org/10.1002/qj.3803.
- IEA (2021), *Methane Tracker*, IEA, Paris. [online] Available from: <https://www.iea.org/reports/methane-tracker-2021> (Accessed 25 February 2022)

- 486 Irakulis-Loitxate, I. et al. (2021), Satellite-based survey of extreme methane emissions in the Permian basin, *Science*
 487 *Advances*, 7(27), eabf4507, doi:10.1126/sciadv.abf4507.
- 488 Irakulis-Loitxate, I., L. Guanter, J. D. Maasakkers, D. Zavala-Araiza, and I. Aben (2022), Satellites Detect Abatable
 489 Super-Emissions in One of the World's Largest Methane Hotspot Regions, *Environ. Sci. Technol.*, 56(4),
 490 2143–2152, doi:10.1021/acs.est.1c04873.
- 491 Lauvaux, T., C. Giron, M. Mazzolini, A. d'Aspremont, R. Duren, D. Cusworth, D. Shindell, and P. Ciais (2022),
 492 Global assessment of oil and gas methane ultra-emitters, *Science*, 375(6580), 557–561,
 493 doi:10.1126/science.abj4351.
- 494 Lin, M., A. M. Fiore, O. R. Cooper, L. W. Horowitz, A. O. Langford, H. Levy II, B. J. Johnson, V. Naik, S. J.
 495 Oltmans, and C. J. Senff (2012), Springtime high surface ozone events over the western United States:
 496 Quantifying the role of stratospheric intrusions, *Journal of Geophysical Research: Atmospheres*, 117(D21),
 497 doi:https://doi.org/10.1029/2012JD018151. [online] Available from:
 498 https://agupubs.onlinelibrary.wiley.com/doi/abs/10.1029/2012JD018151
- 499 Liu, M. et al. (2021), A New Divergence Method to Quantify Methane Emissions Using Observations of Sentinel-
 500 5P TROPOMI, *Geophysical Research Letters*, 48(18), e2021GL094151,
 501 doi:https://doi.org/10.1029/2021GL094151.
- 502 Lyon, D. R. et al. (2021), Concurrent variation in oil and gas methane emissions and oil price during the COVID-19
 503 pandemic, *Atmospheric Chemistry and Physics*, 21(9), 6605–6626, doi:10.5194/acp-21-6605-2021.
- 504 Mayfield, E. N., A. L. Robinson, and J. L. Cohon (2017), System-wide and Superemitter Policy Options for the
 505 Abatement of Methane Emissions from the U.S. Natural Gas System, *Environ. Sci. Technol.*, 51(9), 4772–
 506 4780, doi:10.1021/acs.est.6b05052.
- 507 Olivier, J., and G. Janssens-Maenhout (2012), *CO2 Emissions from Fuel Combustion – 2012 Edition*, IEA CO2
 508 *report 2012, Part III, Greenhouse-Gas Emissions*, OECD Publishing, Paris.
- 509 Robertson, A. M., R. Edie, R. A. Field, D. Lyon, R. McVay, M. Omara, D. Zavala-Araiza, and S. M. Murphy
 510 (2020), New Mexico Permian Basin Measured Well Pad Methane Emissions Are a Factor of 5–9 Times
 511 Higher Than U.S. EPA Estimates, *Environ. Sci. Technol.*, 54(21), 13926–13934,
 512 doi:10.1021/acs.est.0c02927.
- 513 Schneising, O. et al. (2019), A scientific algorithm to simultaneously retrieve carbon monoxide and methane from
 514 TROPOMI onboard Sentinel-5 Precursor, *Atmospheric Measurement Techniques*, 12(12), 6771–6802,
 515 doi:10.5194/amt-12-6771-2019.

- Schneising, O., M. Buchwitz, M. Reuter, S. Vanselow, H. Bovensmann, and J. P. Burrows (2020), Remote sensing of methane leakage from natural gas and petroleum systems revisited, *Atmos. Chem. Phys.*, *20*(15), 9169–9182, doi:10.5194/acp-20-9169-2020.
- Varon, D. J., D. Jervis, J. McKeever, I. Spence, D. Gains, and D. J. Jacob (2021), High-frequency monitoring of anomalous methane point sources with multispectral Sentinel-2 satellite observations, *Atmospheric Measurement Techniques*, *14*(4), 2771–2785, doi:10.5194/amt-14-2771-2021.
- Veefkind, J. P. et al. (2012), TROPOMI on the ESA Sentinel-5 Precursor: A GMES mission for global observations of the atmospheric composition for climate, air quality and ozone layer applications, *rse*, *120*, 70–83, doi:10.1016/j.rse.2011.09.027.
- Warneke, C. et al. (2014), Volatile organic compound emissions from the oil and natural gas industry in the Uintah Basin, Utah: oil and gas well pad emissions compared to ambient air composition, *Atmospheric Chemistry and Physics*, *14*(20), 10977–10988, doi:10.5194/acp-14-10977-2014.
- Zhang, Y. et al. (2020), Quantifying methane emissions from the largest oil-producing basin in the United States from space, *Sci. Adv.*, *6*(17), eaaz5120, doi:10.1126/sciadv.aaz5120.

Figure Captions

- Figure 1. CAMS model (see section 3) CH₄ volume mixing ratio profiles for two nearby locations for 1 October 2020. The blue line represents background conditions and the orange line enhanced CH₄ concentrations in the lower troposphere.
- Figure 2. Illustration of the background correction for data over the Permian region for 6 October 2020. Left panel: CH₄ column concentration plotted as function of the surface pressure (blue points) and the corresponding linear fit (black line). Middle top panel: surface pressure. Right top panel: CH₄ column concentration. Middle bottom panel: background CH₄ column concentration. Right bottom: background corrected CH₄ column concentration.
- Figure 3. Divergence method applied to CAMS model data. Top-left panel: CH₄ emission derived from CAMS model data with the divergence method. Top-right panel: CAMS input emissions on the original resolution. Bottom-left panel: CAMS input emission with a Gaussian blur with $\sigma=0.8$. Bottom-right panel: retrieved emissions plotted as function of the CAMS input emissions, for the original and blurred data.
- Figure 4. Panel top left: Median CH₄ emission derived using the divergence method applied to TROPOMI data from 2019-2020. Top-right NO_x emission for 2018-2020 retrieved from TROPOMI [REF Dix]. Bottom left: production drilling categories. Bottom right, combined violin and boxplot showing the distribution of retrieved CH₄ emissions for each production/drilling category.
- Figure 5. Time series for five locations with high CH₄ emissions. The blue dots are the daily data, the orange line the 30-day running mean and the green line represents the 30-day running median. Running mean and medians are only shown when at least 5 of the 30 days contain valid data. The grey area indicates the interquartile range and the black line the median over the whole time period.

Table Captions

- Table 1. Sensitivity of the emissions for 2020 derived from the CAMS data for the entire domain, for variations in the assumed boundary layer height, the order of the central-finite difference method and the method to compute the background. The first column represents the default case, which uses a boundary layer height of 500m, 4th order central finite difference and a fit of the background concentration based on the 25th percentiles. Variations with respect to the default are a 250 m or 1000m boundary layer height, a 2nd order the central-finite difference method, and a least-squares fit (Ltsq) for the background concentration. The table lists the mean, median, 25th percentile (P1) and 75th percentile (P3) of the difference with the default case.
- Table 2. Annual Emissions derived with the divergence method for the Delaware, Midland sub-basins and for the entire Permian basin for 2019, 2020 and 2019-2020. The Delaware and Midland basins are sub-basins of the Permian (see Figure S3).

Continuous Methane Emissions from the Oil and Gas Industry in the Permian Basin

J. P. Veefkind^{1,2}, R. Serrano-Calvo², J. de Gouw^{3,4}, B. Dix³, O. Schneising⁵, M. Buchwitz⁵, J. Barré⁶,
R. van der A¹, M. Liu¹, P.F. Levelt^{1,2,7}

¹ Royal Netherlands Meteorological Institute KNMI, De Bilt, The Netherlands.

² Delft University of Technology, Dept. Geoscience and Civil Engineering, Delft, The Netherlands.

³ Cooperative Institute for Research in Environmental Sciences, University of Colorado, Boulder, CO, United States.

⁴ Department of Chemistry, University of Colorado, Boulder, CO, United States.

⁵ Institute of Environmental Physics (IUP), University of Bremen FB1, Bremen, Germany.

⁶ University Cooperation for Atmospheric Research, Boulder, CO, United States.

⁷ National Center for Atmospheric Research, Boulder, CO, United States.

Contents of this file

Figures S1 to S4

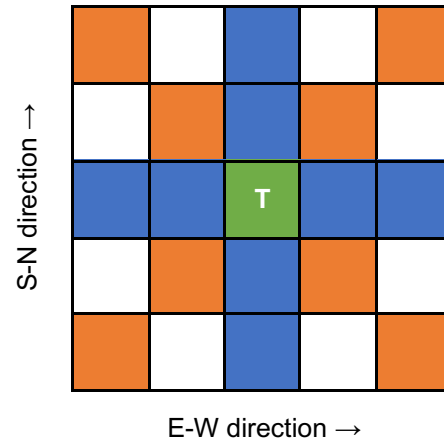


Figure S1. Schematic view of the ground pixels used to compute the divergence. For the green target pixel the standard divergence is computed based on the blue pixels. The rotated divergence is computed based on the orange pixels.

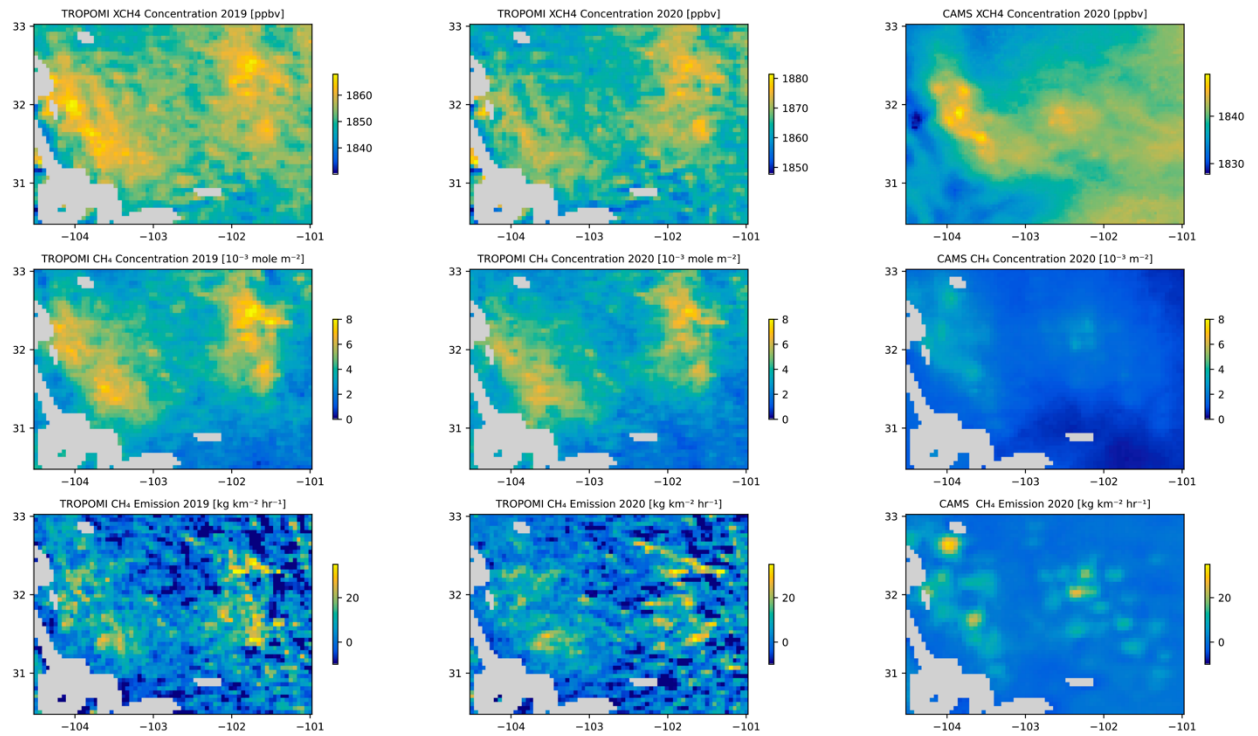


Figure S2. Top row: median XCH₄ for Tropomi for 2019 (left), 2020 (middle) and for the CAMS model data for 2020. Middle row: same as top row, but for the background corrected CH₄ column concentrations. Bottom row: same as top row, but for the CH₄ emissions derived with the divergence method.

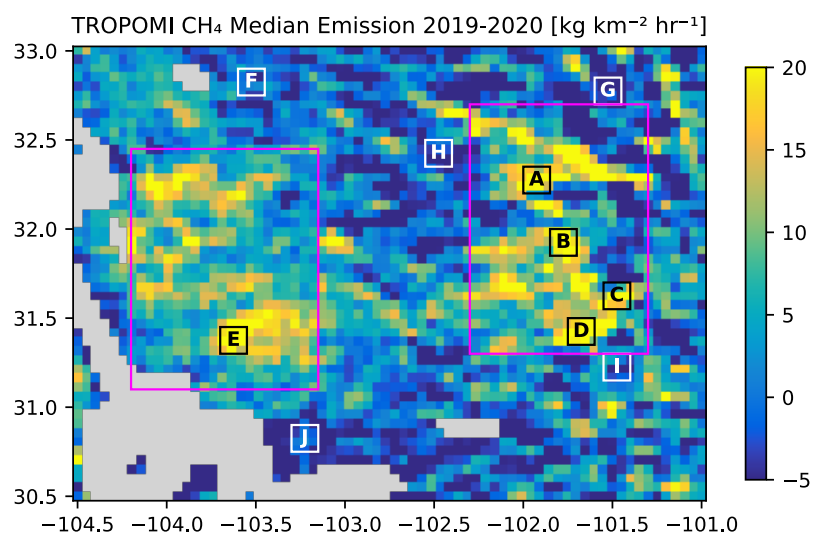


Figure S3. CH₄ median emission with the five selected locations with high emissions (labeled A-E in black) and background emissions (labeled F-J in white). The pink boxes indicate the areas used for computing the statistics for the Delaware and Midland sub-basins

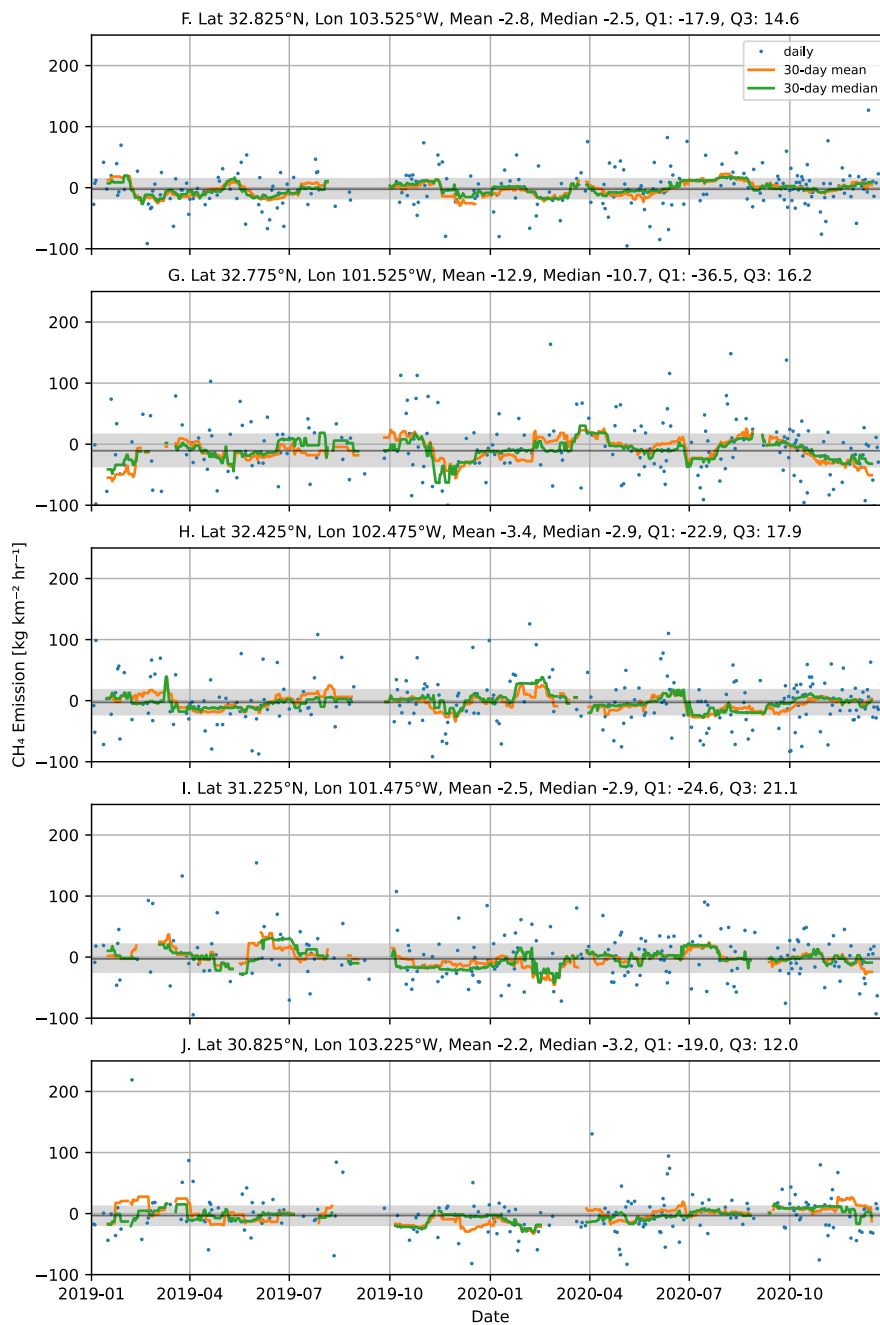


Figure S4. Time series for five locations with background CH₄ emissions. The blue dots are the daily data, the orange line the 30-day running mean and the green line represents the 30-day running median. Running mean and medians are only shown when at least 5 of the 30 days contain valid data. The grey area indicates the interquartile range and the black line the median over the whole time period.